Effect of Cr^{3+} doped on electronic and magnetic properties of $SrFe_{12}O_{19}$ by first-principles study

H'Linh Hmŏk[1,*], I. Betancourt[1], E. Martínez-Aguilar[2], J. Ribas-Ariño[3], O. Raymond Herrera[4]

[1]*Instituto de Investigaciones en Materiales, Universidad Nacional Autónoma de México,Ciudad de México 04510, México*

[2]*Unidad Morelia del Instituto de Investigaciones en Materiales, Universidad Nacional Autónoma de México, Antigua Carretera a Pátzcuaro No. 8701, Col. Ex Hacienda de San José de la Huerta, C.P. 58190 Morelia, Michoacán, México*

[3]*Departament de Ciència de Materials i Química Física and IQTCUB, Universitat de Barcelona, Martí i Franquès 1, 08028 Barcelona, Spain*

[4]*Centro de Nanociencias y Nanotecnología, Universidad Nacional Autónoma de México, Apdo. Postal 14, Ensenada 22860, Baja California, México*

*Corresponding author's email: hlinh.hmok@gmail.com

Abstract

This theoretical work presents the electronic and magnetic properties of Cr-doped $SrFe_{12}O_{19}$ using first-principles calculations based on density functional theory. An improvement in the magnetic properties of $SrFe_{12}O_{19}$ is predicted when doped with the Cr^{3+} ion. It was found that the magnetic Cr^{3+} ion preferentially replaces Fe^{3+} ion at 2a, $4f_1$, and 12k sites. The calculation demonstrates that if Cr ion occupies the $4f_1$ site, a total magnetization of 52.920 emu/g is obtained. On the other hand, $SrFe_{11.5}Cr_{0.5}O_{19}$ behaves as a semiconductor when Cr occupies the 2a and 12k sites while behaves like half-metal when Cr occupies the $4f_1$ site. The higher magnetization, identified for the $SrFe_{11.5}Cr_{0.5}O_{19}$ compound, provides unique qualities in the applications of permanent magnets and/or related devices like spintronics and magnetic semiconductors.

Keywords: electronic structure; magnetism; DFT; hexaferrite

Introduction

The members of the hexaferrite family are well known for their use as permanent magnets, in applications as magnetic recording and data storage materials, and as components in electrical devices, particularly those operating at microwave/GHz frequencies [1]. The M-type hexaferrites of $MFe_{12}O_{19}$ (M = Sr, Ba, Pb) exhibits high saturation magnetization (M_S), coercivity (H_C), Curie temperature, electrical resistivity, uniaxial magnetic anisotropy, and excellent chemical and mechanical stability. [2-4]. Their magnetic properties originate from the high magnetic moment of the Fe^{3+} ions occupying five Wyckoff sites (2a, 2b, $4f_1$, $4f_2$ and 12k) and the magneto-crystalline anisotropy with a single easy magnetization axis [5].

Many experimental works are focused on the effects of the magnetic and electrical properties of $SrFe_{12}O_{19}$ (SFO) doping with other cations such as Ga [6,7] , In [6,7], Sm [8], Nd [9], La [10,11], Pr [12], Zn-Sn [13], Sn-Mg [3], Er-Ni [2], Bi-Cr [14], Nd-Co [15], Al [5], Ce-Zn [16] and Co [17]. However, there are few first-principles studies on doped $SrFe_{12}O_{19}$: in 2003, Fang *et al.* [18] investigated the magnetic and electronic properties of SFO from first-principles calculations, and their calculations showed that the most stable state of the hexaferrite is a ferrimagnetic order with the Fe^{3+} ions at the 4f sites having their magnetic moment anti-parallel to the rest of the Fe^{3+} ions such as Gorter's prediction [19,20]. In 2014, using DFT and generalized gradient approximation (GGA), Park *et al.* calculated the temperature dependence of magnetic moments m(T) for the five sublattices of the 2a, 2b, 12k, $4f_1$, and $4f_2$ sites using the exchange integrals. They found that m(T) for the five sublattices are inter-related to the nearest neighbors, where the magnetic moments are mostly antiferromagnetically coupled [21]. The electronic structure of $La_xSr_{1-x}Fe_{12}O_{19}$ (x = 0, 0.25, 0.5, 0.75, 1) hexaferrite was calculated by P. Novák et al. using the DFT and GGA, and they found that the magnetic moment decreases linearly with the increasing of La content in agreement with the experiment [22]. Liyanage *et al*. studied the magnetic properties of $SrFe_{12-x}(Zn_{0.5}Sn_{0.5})xO_{19}$ with x = 1, using density functional theory (DFT), predicting a rapid increase in saturation magnetization (Ms) as well as a decrease in magnetic anisotropy compared to the pure SFO [23]. Moreover, the site occupancies and

magnetic properties of SFO doped with Al, Sc, Ti, P, Sn, Co, Ni, As, Bi, Sb, Ag, Cu, Ir, Pb, Au, Pt, Pd, Tl, Br, In and Ga have been investigated by Dixit *et al*. [4, 24,25].

On the other hand, K. Praveena et al. [26] and Sadhana Katlakunta et al. [27] reported a Ms decrease and Hc increase with the increase of the Cr^{3+} concentration in $SrFe_{12}O_{19}$. Magnetic hyperfine analysis using the Mössbauer technique indicates that Cr^{3+} ions preferentially occupy 2a, 12k, and $4f_1$ sites [27]. To our knowledge, no first-principles calculation on the electronic and magnetic properties has been yet performed on SFO doping with Cr^{3+}.

Thus, the objective of this work is to investigate theoretically the effects induced by the substitution of Cr^{3+} in the electronic and magnetic properties of $SrFe_{12}O_{19}$ ($SrFe_{11.5}Cr_{0.5}O_{19}$) using the density functional theory. To this end, a detailed analysis of the stable crystal structures resulting from SFO doping with Cr in different interstitial sites will be presented. Electronic properties were explored using the combination of different representations such as the density of electronic states (DOS) and band structure. Magnetic properties are reported in detail. A comparative analysis between the theoretical results and experimental reports is also presented.

Results and discussion

Structural properties

In Fig. 1a) the unit cell of the SFO compound is shown. The magnetism in SFO arises from Fe^{3+} ions that occupy five crystallographic non-equivalent sites in the unit cell, a tetrahedral site ($4f_1$), a trigonal bipyramidal site (2b), and three octahedral sites (2a, 12k, and $4f_2$). The iron ions at the $4f_1$ and $4f_2$ sites have their magnetic moment with orientation antiparallel to that of the iron ions at the 2a, 2b and, 12k sites (Fig. 1b) [6-8].

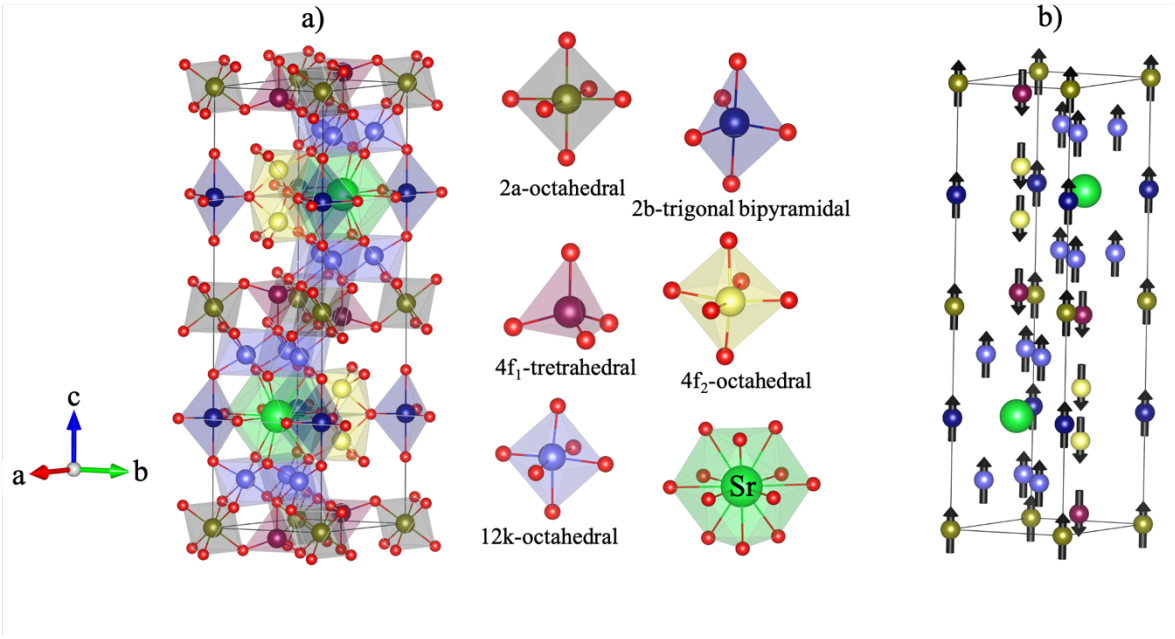

Fig. 1. a) Unit cell of strontium hexaferrite. The red spheres are O atoms and the green spheres are Sr atoms. The Fe ions are at the non-equivalent sites, octahedron (2a), bipyramidal (2b), tetrahedral ($4f_1$), octahedron ($4f_2$) and octahedron (12k). b) the magnetic moment direction of the Fe ions is shown by arrows; the magnetic moments of Fe ions at $4f_1$ and $4f_2$ point downward, and at sites 2a, 2b, and 12k sites point upward. For clarity, O atoms are not shown in b).

For the $SrFe_{11.5}Cr_{0.5}O_{19}$, one of the 24 Fe sites is substituted by a Cr atom of the unit cell. Thus, different $SrFe_{11.5}Cr_{0.5}O_{19}$ unit cells were created, substituting a Fe ion at one of the five non-equivalent sites (2a, 2b, $4f_1$, $4f_2$, or 12k) by a Cr atom and a subsequent full optimization of the unit cell volume and ionic positions. In all relaxation processes and calculation of properties, the magnetic orderings of Fe and Cr were considered. From the self-consistent field calculation, it was identified that the SFO is ferrimagnetic with the Fe ions at the $4f_1$ and $4f_2$ sites having the magnetic moment anti-parallel to the rest of the Fe ions (see Fig. 1b) as reported by Fang in 2005 [18] and the Gorter's prediction [19, 20]. Hereafter, we use the following notations, ↑ is the majority direction (along the positive *c*) and ↓ is the minority direction (along the negative *c*). For example: Fe-$4f_1$-↑ means that iron at the $4f_1$ site has its magnetic moment oriented in the majority direction, that is, in the positive *c* direction. In this work, the convergence of the structural relaxation was obtained in the following configurations: [Fe-2a-↑][Cr-2a-↓] (see Fig. 2a), [Fe-$4f_1$-↓][Cr-$4f_1$-↓] (see Fig. 2b), [Fe-$4f_1$-↓][Cr-$4f_1$-↑] (see Fig. 2c), [Fe-12k-↑][Cr-12k-↑] (see Fig. 2d), and [Fe-12k-↑][Cr-12k-↓] (see Fig. 2e).

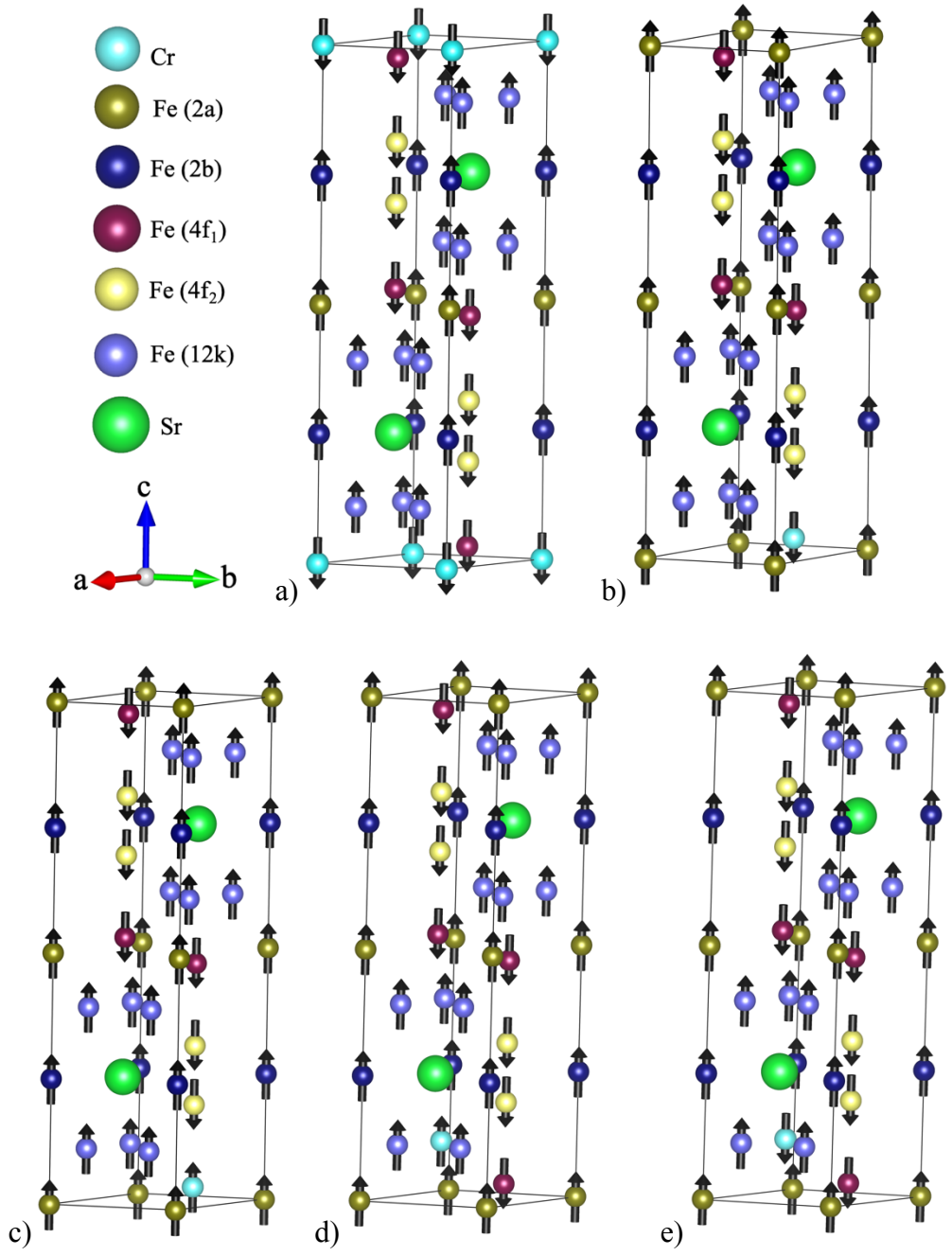

Fig. 2. Unit cell of strontium hexaferrite doped with Cr at different crystallographic sites (here only the most stable spin configurations are shown): a) [Fe-2a-↑][Cr-2a-↓], b) [Fe-4f_1-↓][Cr-4f_1-↓], c) [Fe-4f_1-↓][Cr-4f_1-↑], d) [Fe-12k-↑][Cr-12k-↑] and e) [Fe-12k-↑][Cr-12k-↓].

Table 1 shows the calculated values of the lattice parameters and the unit cell volume of the pure SFO and Cr doped SFO cells illustrated in Fig. 1 and Fig. 2, respectively. The lattice parameters of SFO are slightly larger compared to the reported experiments [14, 28], this is

because the calculation is used generalized gradient approximation (GGA) which is over-estimates lattice parameters. We observed that the substitution of Fe^{3+} ions by Cr^{3+} ions considerably affects the unit cell parameters. As can be seen in Table 1, the unit cell volume of the $SrFe_{11.5}Cr_{0.5}O_{19}$, except for the [Fe-4$f_1$-↓][Cr-4$f_1$-↑] configuration, was smaller than that of $SrFe_{12}O_{19}$ which is in agreement with the experimental results reported in Ref. [27]. This is due to the ionic radius of Fe^{3+} (0.645 Å) is higher than the ionic radius of Cr^{3+} (0.615 Å), both having high spin states on VI coordination [29]. For the [Fe-4f_1-↓][Cr-4f_1-↑] configuration (Fig. 2c), the volume of the unit cell is slightly higher compared with pure SFO, which can be attributed to the local distortion promoted by the Cr incorporation (see below).

On the other hand, as it can see in Table 1, the total energy (E) for the [Fe-12k-↑][Cr-12k-↑] and [Fe-12k-↑][Cr-12k-↓] configurations is the most negative, indicates that the structure of these configurations is more stable than those with [Fe-4f_1-↓][Cr-4f_1-↓], [Fe-4f_1-↓][Cr-4f_1-↑] and [Fe-2a-↑][Cr-2a-↓] configurations.

Table 1. Values of the lattice parameters (a, c), unit cell volume (V) and total energy (E) obtained for all configurations

Configuration	a (Å)	c (Å)	V (Å^3)	E (Ry)
SFO	6.111	23.877	772.176	
[Fe-2a-↑][Cr-2a-↓]	6.105	23.852	769.764	-2411.229
[Fe-4f_1-↓][Cr-4f_1-↓]	6.109	23.868	771.310	-2411.154
[Fe-4f_1-↓][Cr-4f_1-↑]	6.112	23.880	772.474	-2411.133
[Fe-12k-↑][Cr-12k-↑]	6.104	23.849	769.511	-2411.240
[Fe-12k-↑][Cr-12k-↓]	6.104	23.840	769.486	-2411.240

Figs. 3a, 3b, and 3c show the values of the closest Cr-O-Fe bond angles with Cr at 2a, 4f_1, and 12k, respectively, and the distance between Cr or Fe at 2a and Fe at 2b site (Cr/Fe(2a)-Fe(2b)), for doped SFO after structural relaxing in comparison with those corresponding values for pure SFO. It is observed that when Cr occupies the 2a or 12k sites, the Cr-O-Fe bonds angle increases, and the Cr(2a)-Fe(2b) distance decrease compared with those of SFO (see tables in Fig. 3a and 3c). Meanwhile, when the Cr occupies the 4f_1 site, it causes a slight increase Cr-O-Fe bond angle and a decrease of Cr(2a)-Fe(2b) distance for [Fe-4f_1-↓] [Cr-4f_1-↓] configuration; whereas, for the [Fe- 4f_1-↓] [Cr-4f_1-↑] configuration a decrease of the Cr-O-Fe bond angle and an increase of the Cr(2a)-Fe(2b) distance is obtained (table in

Fig. 3b) which, specifically, explain the increase of the *c* parameter and therefore, the increase of the unit cell volume in opposite to the other configurations.

	SFO		[Fe-2a-↑][Cr-2a-↓]
Fe(2a)-O-Fe ($4f_1$) (º)	124.52	Cr(2a)-O-Fe ($4f_1$) (º)	125.82
Fe(2a)-O-Fe(2b) (º)	180.00	Cr(2a)-O-Fe(2b) (º)	180.00
Fe(2a)-O-Fe(12k) (º)	95.72	Cr(2a)-O-Fe(12k) (º)	96.25
Fe(2a)-Fe(2b) (Å)	5.969	Cr(2a)-Fe(2b) (Å)	5.963

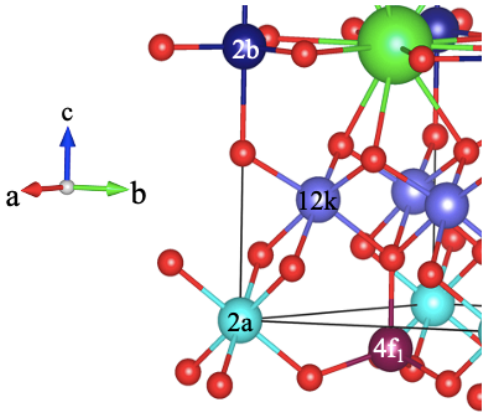

a)

	SFO		[Fe-$4f_1$-↓][Cr-$4f_1$-↓]	[Fe-$4f_1$-↓][Cr-$4f_1$-↑]
Fe($4f_1$)-O-Fe(2a) (º)	124.53	Cr($4f_1$)-O-Fe(2a) (º)	125.74	124.48
Fe($4f_1$)-O-Fe(12k) (º)	121.28	Cr($4f_1$)-O-Fe(12k) (º)	121.36	120.79
Fe(2a)-Fe(2b) (Å)	5.969	Fe(2a)-Fe(2b) (Å)	5.967	5.970

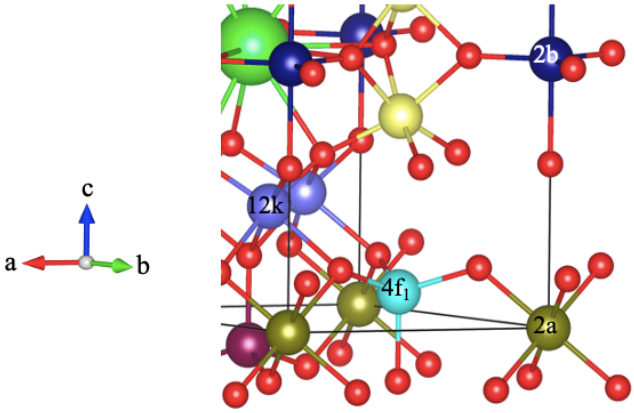

b)

	SFO		[Fe-12k-↑][Cr-12k-↑]	[Fe-12k-↑][Cr-12k-↓]
Fe(12k)-O-Fe(2a) (º)	95.72	Cr(12k)-O-Fe(2a) (º)	95.06	94.48
Fe(12k)-O-Fe(2b) (º)	120.02	Cr(12k)-O-Fe(2b) (º)	122.99	122.48
Fe(12k)-O-Fe($4f_1$) (º)	121.28	Cr(12k)-O-Fe($4f_1$) (º)	121.75	121.86
Fe(12k)-O-Fe($4f_2$) (º)	126.87	Cr(12k)-O-Fe($4f_2$) (º)	128.46	127.78
Fe(12k)-O-Fe(12k) (º)	97.89	Cr(12k)-O-Fe(12k) (º)	99.18	99.15
Fe(2a)-Fe(2b) (Å)	5.969	Fe(2a)-Fe(2b) (Å)	5.962	5.960

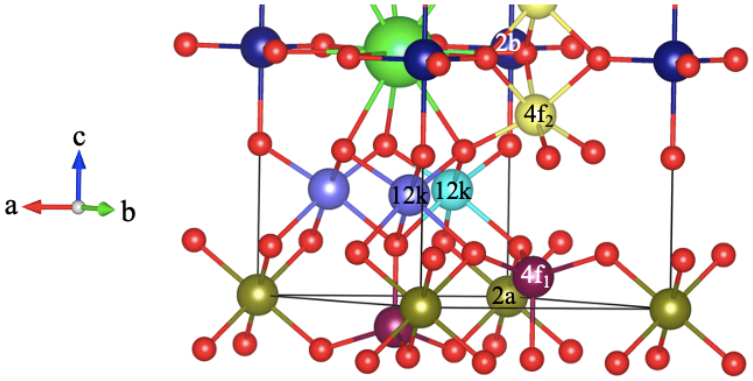

c)

Fig. 3. Local changes produced in the Cr/Fe-O-Fe bond angle after structural relaxation compared with SFO for a) [Fe-2a-↑][Cr-2a-↓], b) [Fe-$4f_1$-↓][Cr-$4f_1$-↓] and [Fe-$4f_1$-↓][Cr-$4f_1$-↑], c) [Fe-12k-↑][Cr-12k-↑] and [Fe-12k-↑][Cr-12k-↓]. The atom legend is the same as in Fig. 1.

Magnetic properties

The tables 2, 3, and 4 exhibit the magnetic moment values of all atoms and the total magnetization obtained from the self-consistent calculations for pure SFO and Cr doped SFO in the five configurations with Cr occupying the 2a, $4f_1$, and 12k sites, respectively. As mentioned above, the calculations only converged the configurations with Cr at 2a, $4f_1$, and 12k sites, which is in good agreement with the experimental results reported in Ref. [27]. The most important contribution of the magnetic moments comes from Fe and Cr atoms, which is related to the half *d* band filling. In all compounds, pure and doped, the Fe^{3+} ions have magnetic moment values between 3.87 μ_B and 4.07 μ_B, while the Cr^{3+} ions have magnetic moment values between 2.25 μ_B and 2.59 μ_B (Tables 2-4). It is identified that Cr doping produces a reduction or an increase in the total magnetization ($\sum m$) compared with the pure $SrFe_{12}O_{19}$, depending on the crystallography site occupied by the Cr ion. When the Cr^{3+} ion replaces the Fe^{3+} ion at the minority $4f_1$ site with magnetic moment along to *c* negative, it eliminates a negative contribution and hence increases the total magnetization from 44.572 emu/g for pure SFO to 47.076 emu/g for the [Fe-$4f_1$-↓][Cr-$4f_1$-

↓] configuration (shown in Fig. 2b) and to 52.920 emu/g for the [Fe-4f_1-↓][Cr-4f_1-↑] configuration (shown in Fig. 2c). On the other hand, when the Cr^{3+} ion replaces the Fe^{3+} ion at the majority 2a and 12k sites with magnetic moment along *c* positive, it eliminates a positive contribution and reduces the total magnetic moment. Thus, the total magnetization decrease to 35.953 emu/g for the [Fe-2a-↑][Cr-2a-↓] configuration (shown in Fig. 2a), to 42.010 emu/g for the [Fe-12k-↑][Cr-12k-↑] configuration (shown in Fig. 2d) and to 36.041 emu/g for the [Fe-12k-↑][Cr-12k-↓] configuration (shown in Fig. 2e).

In this work, all total magnetization values, are higher than those experimental value of 29 emu/g reported for $SrFe_{11.5}Cr_{0.5}O_{19}$ powders obtained by sol-gel in the Ref. [27]. This difference, compared with those reported in this work, may be due to the random incorporation of the Cr^{3+} ions in all possible sites, the presence of different types of structural defects, and the spin glass structure at the grain boundaries of the $SrFe_{11.5}Cr_{0.5}O_{19}$ powders characterized by its polycrystalline nature.

In summary, this result shows that if the Cr^{3+} ion occupies the $4f_1$ site, an increase in total magnetization is obtained compared with the pure SFO, which opens up the possibility to increase total magnetization improving the potential application of $SrFe_{12}O_{19}$ for permanent magnets.

Table 2. values of the magnetic moment of all atoms in the unit cells and the total magnetization ($\sum m$) of the pure SFO and Cr doped SFO at 2a site. Δm, is the difference between the values of SFO and Cr doped SFO.

Site	SFO		[Fe-2a-↑][Cr-2a-↓]		
	Ion	m (μ_B)	Ion	m (μ_B)	Δm
2d	2 Sr	-0.0054	2 Sr	-0.0052	0.0002
2a	1 Fe	4.0730	1 Fe	4.0726	-0.0004
	1 Fe	4.0730	1 Cr	-2.4963	-6.5693
2b	2 Fe	7.7726	2 Fe	7.7578	-0.0148
$4f_1$	4 Fe	-15.6292	4 Fe	-15.6550	-0.0258
$4f_2$	4 Fe	-16.1612	4 Fe	-16.1668	-0.0056
12k	12 Fe	48.0036	12 Fe	47.9797	-0.0239
4e	4 O	1.2800	4 O	1.2900	0.0100
4f	4 O	0.3272	4 O	0.2986	-0.0286
6h	6 O	0.0120	6 O	-0.0436	-0.0556
12k	12 O	1.0404	12 O	0.6698	-0.3706
12k	12 O	1.9056	12 O	1.8950	-0.0106
	$\sum m$ (μ_B)	36.6916	$\sum m$ (μ_B)	29.5966	-7.095
	$\sum m$ (emu/g)	44.572	$\sum m$ (emu/g)	35.953	-8.619

Table 3. Value of the magnetic moment of all atoms in the unit cells and the total magnetization ($\sum m$) of the pure SFO and Cr doped SFO with Cr at $4f_1$ site. Δm, is the difference between the values of SFO and Cr doped SFO.

Site	SFO		[Fe-$4f_1$-↓][Cr-$4f_1$-↓]			[Fe-$4f_1$-↓][Cr-$4f_1$-↑]		
	Ion	m (μ_B)	Ion	m (μ_B)	Δm	Ion	m (μ_B)	Δm
2d	2 Sr	-0.0054	2 Sr	-0.0053	0.0001	2 Sr	-0.0052	0.0002
2a	2 Fe	8.1460	2 Fe	8.1164	-0.0296	2 Fe	8.1576	0.0116
2b	2 Fe	7.7726	2 Fe	7.7712	-0.0014	2 Fe	7.7755	0.0029
$4f_1$	1 Fe	-3.9073	1 Cr	-2.2537	1.6536	1 Cr	2.5893	6.4966
	3 Fe	-11.7219	3 Fe	-11.7206	0.0013	3 Fe	-11.7128	0.0091
$4f_2$	4 Fe	-16.1612	4 Fe	-16.1544	0.0068	4 Fe	-16.1618	-0.0006
12k	12 Fe	48.0036	12 Fe	47.9472	-0.0564	12 Fe	48.0384	0.0348
4e	4 O	1.2800	4 O	1.2945	0.0145	4 O	1.2932	0.0132
4f	4 O	0.3272	4 O	0.4411	0.1139	4 O	0.3968	0.0696
6h	6 O	0.0120	6 O	0.0156	0.0036	6 O	0.0102	-0.0018
12k	12 O	1.0404	12 O	1.3932	0.3528	12 O	1.2749	0.2345
12k	12 O	1.9056	12 O	1.9077	0.0021	12 O	1.9080	0.0024
	$\sum m$ (μ_B)	36.6916	$\sum m$ (μ_B)	38.7529	2.0613	$\sum m$ (μ_B)	43.5641	6.8725
	$\sum m$ (emu/g)	44.572	$\sum m$ (emu/g)	47.076	2.504	$\sum m$ (emu/g)	52.920	8.348

Table 4. Values of the magnetic moment of all atoms in the unit cells and the total magnetization ($\sum m$) of the pure SFO and Cr doped SFO with Cr at 12k site. Δm is the difference between the values of SFO and Cr doped SFO.

Site	SFO		[Fe-12k-↑][Cr-12k-↑]			[Fe-12k-↑][Cr-12k-↓]		
	Ion	m (μ_B)	Ion	m (μ_B)	Δm	Ion	m (μ_B)	Δm
2d	2 Sr	-0.0054	2 Sr	-0.0045	0.0009	2 Sr	-0.006	-0.0006
2a	2 Fe	8.1460	2 Fe	8.1358	-0.0102	2 Fe	8.1318	-0.0142
2b	2 Fe	7.7726	2 Fe	7.7478	-0.0248	2 Fe	7.7453	-0.0273
$4f_1$	4 Fe	-15.6292	4 Fe	-15.5795	0.0497	4 Fe	-15.6261	0.0031
$4f_2$	4 Fe	-16.1612	4 Fe	-16.1059	0.0553	4 Fe	-16.1165	0.0447
12k	1 Fe	4.0003	1 Cr	2.3798	-1.6205	1 Cr	-2.4321	-6.4324
	11 Fe	44.0033	11 Fe	43.9752	-0.0281	11 Fe	43.9179	-0.0854
4e	4 O	1.2800	4 O	1.1785	-0.1015	4 O	1.1853	-0.0947
4f	4 O	0.3272	4 O	0.2986	-0.0286	4 O	0.2748	-0.0524
6h	6 O	0.0120	6 O	0.0007	-0.0113	6 O	-0.0054	-0.0174
12k	12 O	1.0404	12 O	0.9192	-0.1212	12 O	0.9270	-0.1134
12k	12 O	1.9056	12 O	1.6596	-0.246	12 O	1.6727	-0.2329
	$\sum m$ (μ_B)	36.6916	$\sum m$ (μ_B)	34.5827	-2.1089	$\sum m$ (μ_B)	29.6687	-7.0229
	$\sum m$ (emu/g)	44.572	$\sum m$ (emu/g)	42.010	-2.562	$\sum m$ (emu/g)	36.041	-8.531

Electronic structure

The calculation of the projected density of states (PDOS) of Fe-3*d* (at 2a, 2b, $4f_1$, $4f_2$, 12k sites) and O-2*p* orbitals, and the total density of states (TDOS) of pure SFO are shown in

Fig. 4a, where it is identified that the *spin up* (positive values of the density of states) and *spin down* (negative values of the density of states) states do not show symmetry. Such asymmetries in the electronic properties are particularly related to the magnetic properties of ferrimagnetic ordering. This magnetism arises from the fact that electronic states degeneracy is broken, and there are more electrons with *spin up* than electrons with *spin down*. The hybridization between Fe-3*d* and O-2*p* occurs in all valence band (VB) energy ranges. As can be seen, the PDOS profiles of the 3*d* orbital of Fe at 2a, $4f_2$, and 12k sites are different between them, which can be due to distortions of the FeO_6 octahedra with different Fe-O bond lengths (see Fig. S1 and Table S1 in the supplementary material). The hybridization between Fe-3*d* and O-2*p* is principally due to Fe ions occupying the 2b and 12k sites at the Fermi level. Fig. 4a shows that the maximum of the valence band and the minimum of the conduction band are dominated by O-2*p* and Fe-3*d* states, respectively. The Fig. 4b shows the band structure of *spin up* (left side) and *spin down* (right side) of SFO. Thus, a direct bandgap value of 1.76 eV and an indirect bandgap values of 1.70 eV were obtained, for the respective spin configurations. These results agree with the experimental value previously reported in Ref. [30], where the direct bandgap energy was determined to be 1.70 eV. Another experimental direct bandgap energy is ~ 1.89 eV reported by [31]. In this work, we highlight the values of direct and indirect bandgap energies to give more advantage of the potential of doped SFO for applications in microelectronics and spintronics devices.

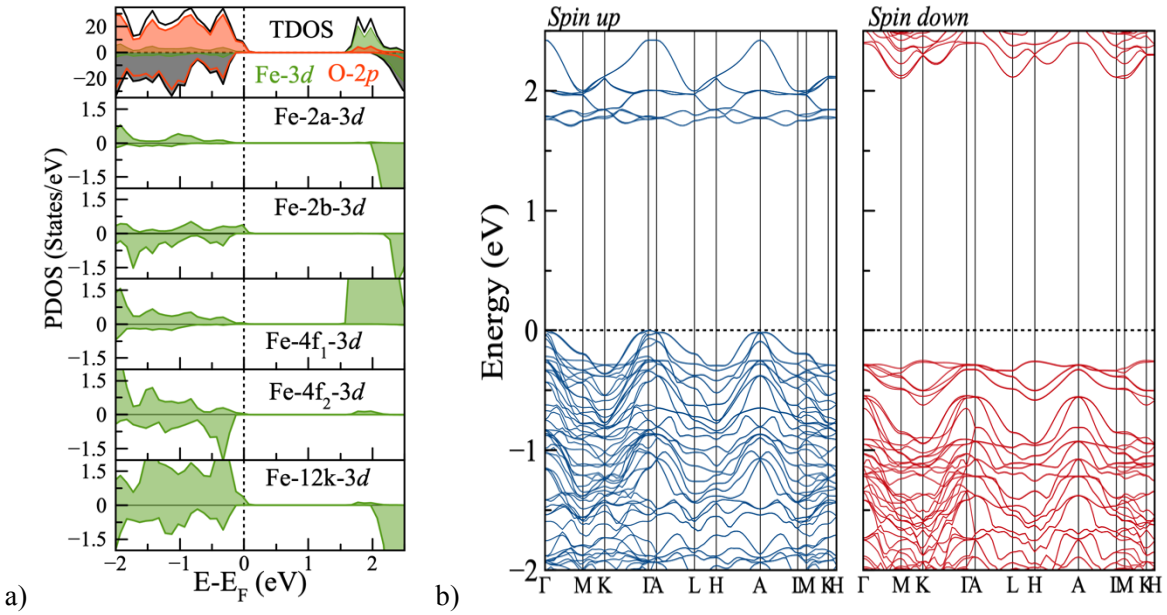

a) b)

Fig. 4. a) TDOS and PDOS (for the Fe-3*d* at 2a, 2b, $4f_1$, $4f_2$, 12k sites and O-2*p* orbitals) and b) band structure for pure SFO.

Fig. 5a shows the selected density of states obtained for the SFO doped with Cr at the 2a site ([Fe-2a-↑][Cr-2a-↓] configuration). In comparison with Fig. 4a for pure SFO, the first evident observation is the introduction of the Cr-3*d* states near below the Fermi level, which states are majority with *spin down*. In the *spin down* states, the states produce a shift in the Fermi level without causing considerable changes in the Fe-3*d* states, so the O-2*p* states present the main interaction with the Cr-2a-3*d* ion. Thus, the bandgap continues to be dominated by the O-2*p* states in the valence band and the Fe-3*d* states in the conduction band. A reduction in the indirect bandgap is manifested, from 1.70 eV for pristine SFO to 1.30 eV for [Fe-2a-↑][Cr-2a-↓] configuration (see Fig. 5b); however, the semiconductor behavior persists.

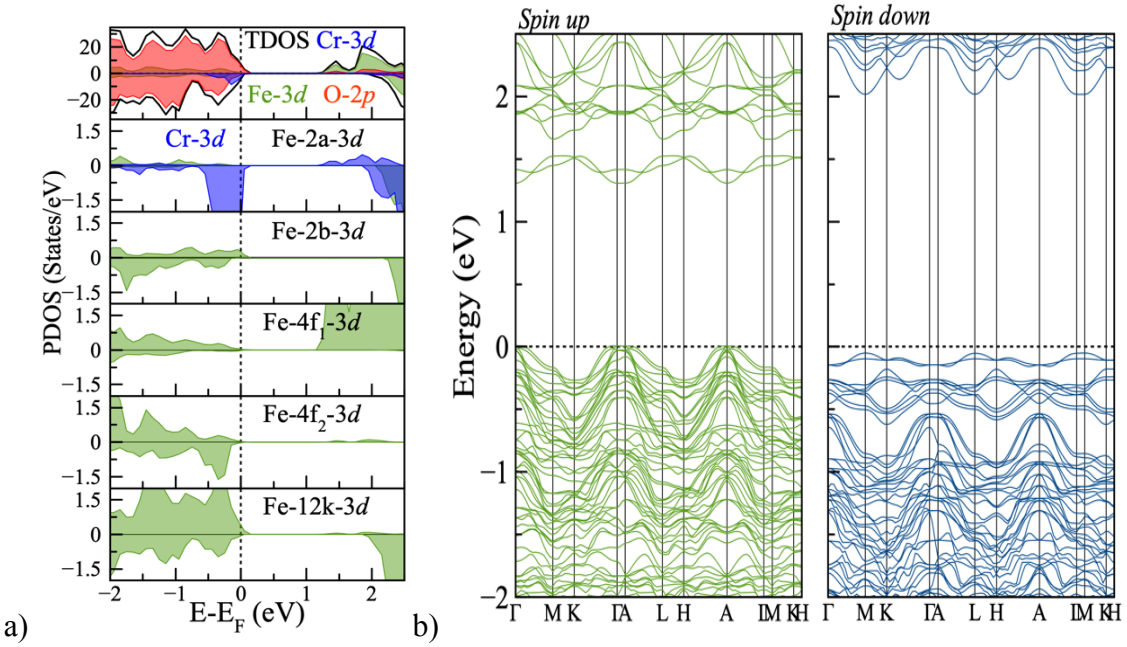

Fig. 5. a) TDOS and PDOS (for the Cr-3*d* at 2a site, Fe-3*d* at 2a, 2b, $4f_1$, $4f_2$, 12k sites and O-2*p* orbitals) and b) band structure for the [Fe-2a-↑][Cr-2a-↓] configuration.

In Fig. 6a, the TDOS and PDOS of SFO doped with Cr at $4f_1$ site ([Fe-$4f_1$-↓][Cr-$4f_1$-↓] configuration) are shown. In this case, the electronic structure is distinguished by the states of Cr-$4f_1$-3*d* introduced at Fermi level with *spin down*. It can be noted that Cr-$4f_1$-3*d* has a low interaction with the Fe-3*d* states at the Fermi level, which indicates electronic exchange

between the Fe-3*d* and Cr-3*d* states mediated by the O-2*p* states. A noticeable indirect bandgap of 1.71 eV is observed for the *spin up* states where the O-2*p* states govern the valence band, while the Fe-3*d* states dominate the conduction band (see Fig. 6b, left side). In the case of the *spin down* states, the presence of Cr-3*d* orbitals from -0.25 eV below the Fermi level to 0.28 eV above the Fermi level (see Fig. 6a) confer a metallic character to the *spin down* states (see Fig. 6b), therefore the solid solution behaves as a half-metal. Thus, the introduction of Cr at $4f_1$ site ([Fe-$4f_1$-↓][Cr-$4f_1$-↓] configuration) gives a ferrimagnetic material with high total magnetization (47.076 emu/g) and spin-polarized half-metal behavior which makes this compound a promising candidate for Spintronics as a source of spin-polarized electron current.

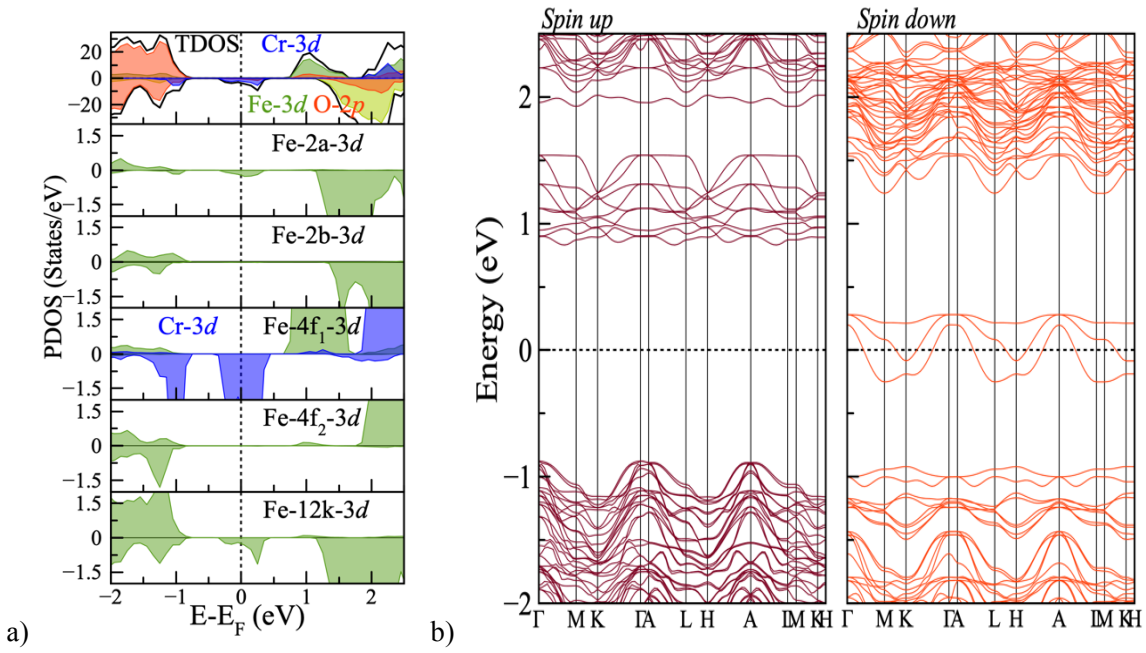

Fig. 6. a) TDOS and PDOS (for the Cr-3*d* at $4f_1$ site, Fe-3*d* at 2a, 2b, $4f_1$, $4f_2$, 12k sites and O-2*p* orbitals and b) band structure for the [Fe-$4f_1$-↓][Cr-$4f_1$-↓] configuration.

When the occupation of Cr is at $4f_1$ site according to the [Fe-$4f_1$-↓][Cr-$4f_1$-↑] configuration, conspicuous changes are observed in the TDOS and PDOS profiles (see Fig. 7a) in comparison with the results for the [Fe-$4f_1$-↓][Cr-$4f_1$-↓] configuration. As a similarity, the Cr-$4f_1$-3*d* states are introduced at Fermi level but with *spin up*, and it can be noted a low

interaction between the Cr-4f$_1$-3*d* and Fe-3*d* states at the Fermi level, which suggest electronic exchange between them are mediated by the O-2*p* states. However, a higher indirect bandgap of 2.26 eV is observed for the *spin down* states where the O-2*p* states govern the valence band, while the Fe-3*d* states dominate the conduction band (see Fig. 7b, right side). On the other hand, the presence of Cr-3*d* orbitals at the Fermi level, from 0.23 eV above the Fermi level to -0.31 eV below the Fermi level (see Fig. 7a), confer a metallic character to the *spin up* states (see Fig. 7b). Therefore, the solid solution behaves as a half-metal. Thus, the introduction of Cr at 4f$_1$ site in the [Fe-4f$_1$-↓][Cr-4f$_1$-↑] configuration gives a ferrimagnetic material with the higher total magnetization (52.920 emu/g) and *spin up*-polarized half-metal behavior which foresee high potential for permanent magnets and magnetoelectric devices for Spintronics.

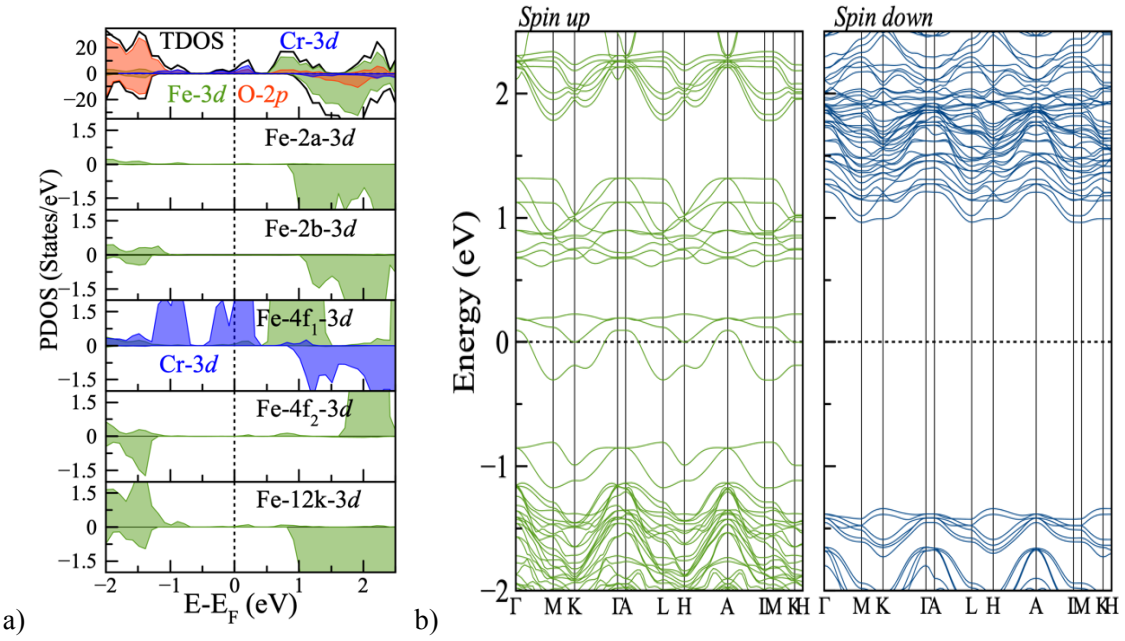

Fig. 7. a) TDOS and PDOS (for the Cr-3*d* at 4f$_1$ site, Fe-3*d* at 2a, 2b, 4f$_1$, 4f$_2$, 12k sites and O-2*p* orbitals) and b) band structure for the [Fe-4f$_1$-↓][Cr-4f$_1$-↑] configuration.

Fig. 8a illustrates that the incorporation of Cr at the 12k site in the [Fe-12k-↑][Cr-12k-↑] configuration produces a shift in the Fermi level, which establishes a direct bandgap of a 0.94 eV (see Fig. 8b) and providing a semiconductor character of this solid solution of Cr-doped SFO. Besides, the magnetic order is affected which can be due by the electronic exchange between the Cr-12k-3*d* and Fe-4f$_1$-3*d* states, again mediated by the O-2*p* states.

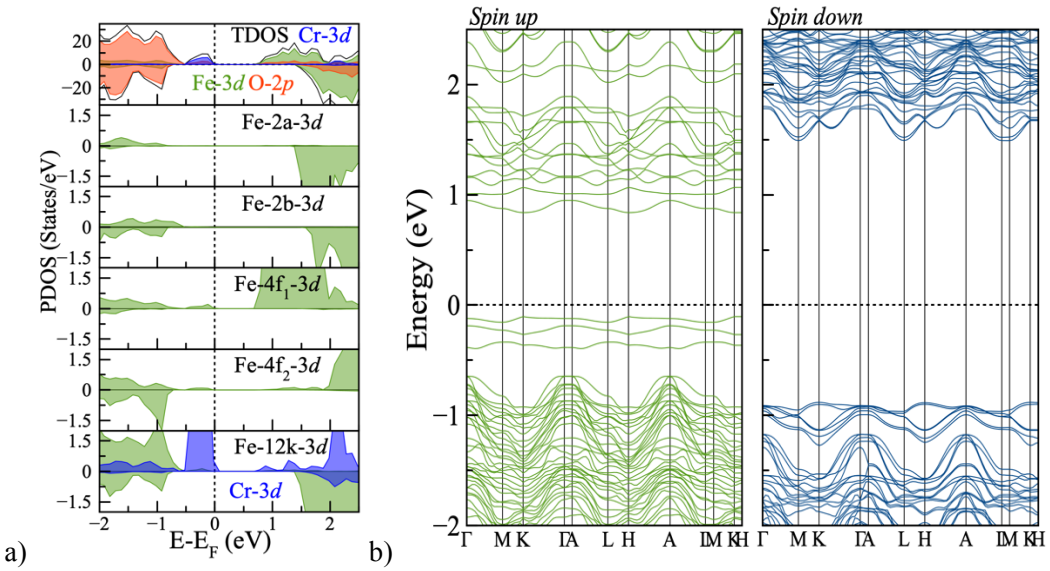

Fig. 8. a) TDOS and PDOS (for the Cr-3*d* at 12k site, Fe-3*d* at 2a, 2b, $4f_1$, $4f_2$, 12k sites and O-2*p* orbitals) and b) band structure for the Fe-12k-↑][Cr-12k-↑] configuration.

Finally, when Cr occupies the 12k site in the [Fe-12k-↑][Cr-12k-↓] configuration, the Cr undergoes a contraction in the distribution of its 3*d* states (see Fig. 9a). This is more noticeable for the *spin down* states in the TDOS, where Cr-3*d* is dominant in the valence band, while at the bottom of the conduction band, the Fe-3*d* states are the majority. This configuration presents an indirect bandgap of 0.97 eV (see Fig. 9b). For this configuration, the applications in magnetic-semiconductor devices can be benefited.

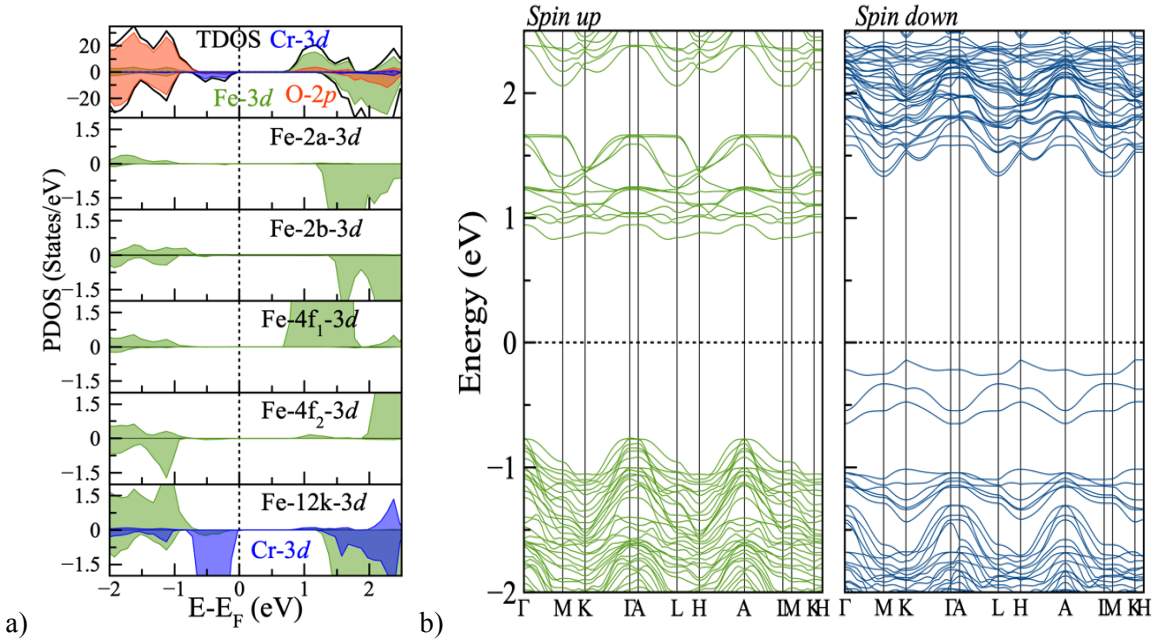

Fig. 9. a) TDOS and PDOS (for the Cr-3*d* at 12k site, Fe-3*d* at 2a, 2b, $4f_1$, $4f_2$, 12k sites and O-2*p* orbitals) and b) band structure for the [Fe-12k-↑][Cr-12k-↓] configuration.

Conclusions

On the basis of density functional theory calculations, the stable configurations and magnetic structures of $SrFe_{12}O_{19}$ and $SrFe_{11.5}Cr_{0.5}O_{19}$ were studied. The influence of Cr on the electronic and magnetic properties of SFO has been revealed. For the solid solution of $SrFe_{11.5}Cr_{0.5}O_{19}$, the doping Cr ion occupies the 2a, $4f_1$, and 12k sites preferentially. Although, the doping of Cr hardly produces effects on the structure of SFO, significant changes in the electronic structure. $SrFe_{11.5}Cr_{0.5}O_{19}$ behaves as a semiconductor when Cr occupies the 2a and 12k sites, while it behaves like half-metal when Cr occupies the $4f_1$ site. The calculation demonstrates that if Cr ion occupies the $4f_1$ site, a total magnetization of 52.920 emu/g is obtained, which foresee the high potential for permanent magnets and magnetoelectric devices for Spintronics.

Computational details

All simulations have been performed with the DFT that implementing in the Quantum-Espresso package [32]. Norm-conserving pseudopotentials were constructed with the generalized gradient approximation (GGA) in the Perdew-Burke-Ernzerhof (PBE) framework, used for exchange-correlation purposes [33-34]. For a correct description of the pseudopotentials, 16 valence electrons were used in Fe ($3s^2 3p^6 3d^6 4s^2$), 6 for O ($2s^2 2p^4$), 10 for Sr ($4s^2 4p^6 5s^2$), and 14 for Cr ($3s^2 3p^6 3d^4 4s^2$). For the energy of the ground state, cut-off energy of 55 Ry was used for the SFO and the Cr doped SFO structures. For all structures, a 4×4×1 mesh was used for geometric optimization, and 8×8×2 *k*-point meshes were used for electronic calculations. The optimization of atomic positions and lattice parameters were performed until the change residual energy and the force acting on each atom were less than 10^{-4} Ry/atom and 10^{-3} Ry/a.u., respectively.

Acknowledgments

The authors thank DGTIC-UNAM for supercomputing support through Project LANCAD-UNAM-DGTIC-236 and Project LANCAD-UNAM-DGTIC-351. H´Linh Hmŏk thanks to DGAPA-UNAM for Scholarship grant No. CJIC/CTIC/1121/2020. E. Martínez-Aguilar thanks to DGAPA-UNAM for Scholarship grant No. CJIC/CTIC/1122/2020.

Declaration of Competing Interest

The authors declare that they have no known competing financial interests or personal relationships that could have appeared to influence the work reported in this paper.

Data availability statement

The data that support the findings of this study are available from the corresponding author upon reasonable request.

References

[1] R. C. Pullar (2012) Prog. Mater. Sci. 57, 1191–1334 http://dx.doi.org/10.1016/j.pmatsci.2012.04.001

[2] M.N. Ashiq, M.J. Iqbal, M. Najam-ul-Haq, P.H. Gomez, A.M. Qureshi (2012) J. Magn. Magn. Mater. 324, 15–19 https://doi.org/10.1016/j.jmmm.2011.07.016

[3] A. Davoodi, B. Hashemi (2011) J. Alloys Compd. 509, 5893–5896 https://doi.org/10.1016/j.jallcom.2011.03.002

[4] V. Dixit, S.G. Kim, J. Park, Y.K. Hong (2017) AIP Adv. 7, 115209 https://doi.org/10.1063/1.4995309

[5] H.Z. Wang, B. Yao, Y. Xu, Q. He, G.H. Wen, S.W. Long, J. Fan, G.D. Li, L. Shan, B. Liu, L.N. Jiang, L.L. Gao (2012) J. Alloys Compd. 537, 43–49 http://dx.doi.org/10.1016/j.jallcom.2012.05.063

[6] G. K. Thompson, B.J. Evans (1994) J. Appl. Phys. 75, 6643 http://dx.doi.org/10.1063/1.356881

[7] T.M. Clark, B.J. Evans, G.K. Thompson, S. Freeman (1999) J. Appl. Phys. 85, 5229 http://dx.doi.org/10.1063/1.369952

[8] J.F. Wang, C.B. Ponton, I.R. Harris (2001) J. Magn. Magn. Mater. 234, 233-240 https://doi.org/10.1016/S0304-8853(01)00366-3

[9] J.F. Wang, C.B. Ponton, I.R. Harris (2002) IEEE Trans. Magn. 38, 2928-2930 https://doi.org/10.1109/TMAG.2002.803071

[10] J.F. Wang, C.B. Ponton, R. Grössinger, I.R. Harris (2004) J. Alloys Compd. 369, 170-177 https://doi.org/10.1016/j.jallcom.2003.09.097

[11] D. Seifert, J. Töpfer, F. Langenhorst, J.-M.L. Breton, H. Chiron, L. Lechevallier (2009) J. Magn. Magn. Mater. 321, 4045-4051 https://doi.org/10.1016/j.jmmm.2009.07.088

[12] J.F. Wang, C.B. Ponton, I.R. Harris (2005) J. Alloys Compd. 403, 104-109 https://doi.org/10.1016/j.jallcom.2005.05.025

[13] A. Ghasemi, V. Sepelák, X. Liu, and A. Morisako (2010) J. Appl. Phys. 107, 09A734 http://dx.doi.org/10.1063/1.3338988

[14] S. Shakoor, M.N. Ashiq, M.A. Malana, A. Mahmood, M.F. Warsi, M. Najam-ul-Haq, N. Karamat (2014) J. Magn. Magn. Mater. 362, 110-114 http://dx.doi.org/10.1016/j.jmmm.2014.03.038

[15] Z. Zhou, Z. Wang, X. Wang, Q. Li, M. Jin, J. Xu (2015) J. Supercond. Nov. Magn. 28, 1773-1778 https://doi.org/10.1007/s10948-014-2920-6

[16] N. Yasmin, M.Z. Iqbal, M. Zahid, S.F. Gillani, M.N. Ashiq, I. Inam, S. Abdulsatar, M. Safdar, M. Mirza (2019) Ceram. Int. 45(7), 462-46 https://doi.org/10.1016/j.ceramint.2018.09.190

[17] H.H. Nguyen, N. Tran, T.L. Phan, D.S. Yang, N.T. Dang, B.W. Lee (2020) Ceram. Int., 46, 19506-19513 https://doi.org/10.1016/j.ceramint.2020.04.304

[18] C. Fang, F. Kools, R. Metselaar, G. de With, R.A. de Groot (2003) J. Phys: Condens. Matter 15, 6229-6237 https://doi.org/10.1088/0953-8984/15/36/311

[19] H. Kojima (1982) Ferromagnetic Materials vol 3, ed E P Wohlfarth (Amsterdam: North-Holland) pp. 305.

[20] E. F. Gorter (1957) Proc. IEEE, 104B, 255S.

[21] J. Park, Y.K. Hong, S.G. Kim, S. Kim, L.S.I. Liyanage, J. Lee, W. Lee, G.S. Abo, K.H. Hur, S.Y. An (2014) J. Magn. Magn. Mater. 355, 1-6 http://dx.doi.org/10.1016/j.jmmm.2013.11.032

[22] P. Novák, K. Knízek, M. Küpferling, R. Grössinger, M.W. pieper (2005) Eur. Phys. J. B 43, 509-515 https://doi.org/10.1140/epjb/e2005-00084-8

[23] L.S.I Liyanage, S. Kim, Y.K. Hong, J.H. Park, S.C. Erwin, S.G. Kim (2013) J. Magn. Magn. Mater. 348, 75-81 http://dx.doi.org/10.1016/j.jmmm.2013.08.006

[24] V. Dixit, C.N. Nandadasa, S.G. Kim, S. Kim, J. Park, Y.K. Hong, L.S.I. Liyanage, A. Moitra (2015) J. Appl. Phys. 117, 243904 http://dx.doi.org/10.1063/1.4922867

[25] V. Dixit, C.N. Nandadasa, S.G. Kim, S. Kim, J. Park, Y.K. hong (2015) J. Appl. Phys. 118, 203908 http://aip.scitation.org/toc/jap/118/20

[26] K. Praveena, M. Bououdina, M. Penchal Reddy, S. Srinath, R. Sandhya, S. Katlakunta (2015) J. Electron. Mater. 44, 524–531 https://doi.org/10.1007/s11664-014-3453-2

[27] S. Katlakunta, S.S. Meena, S. Srinath, M. Bououdina, R. Sandhya, K. Praveena (2015) Mater. Res. Bull. 63, 58-66 https://doi.org/10.1016/j.materresbull.2014.11.043

[28] V. Barrera, I. Betancourt (2016) J. Phys. Chem. Solids 93 (2016) 1–6 https://doi.org/10.1016/j.jpcs.2016.02.007

[29] R.D. Shannon (1976) Acta Crys. A 32 (5), 751–767 https://doi.org/10.1107/S0567739476001551

[30] D.D. Mishra, G. Tan (2018) J. Phys. Chem. Solids 123, 157-161 https://doi.org/10.1016/j.jpcs.2018.07.018

[31] M. Manikandan, K.S. Kumar, N. Aparnadevi, C. Venkateswaran (2015) Phys. Status Solidi A 212, 2179–2185 https://doi.org/10.1002/pssa.201532229

[32] P. Giannozzi, et al. (2009) J. Phys. Condens. Matter 21 (39), 395502 https://doi.org/10.1088/0953-8984/21/39/395502

[33] A.M. Rappe, K.M. Rabe, E. Kaxiras, J.D. Joannopoulos (1990) Phys. Rev. B 41, 1227–1230 https://doi.org/10.1103/PhysRevB.41.1227

[34] N.J. Ramer, A.M. Rappe (1999) Phys. Rev. B 59, 12471–12478 https://doi.org/10.1103/PhysRevB.59.12471